Applied Catalysis A, General 675 (2024) 119639

Contents lists available at ScienceDirect

Applied Catalysis A, General

journal homepage: www.elsevier.com/locate/apcata

Development of an Ir/TiO_2 catalytic coating for plasma assisted hydrogenation of CO_2 to CH_4

Joseph W. Gregory [a], Nima Pourali [a,*], Yuyan Gong [a], Richard I. Walton [b], Volker Hessel [a,c], Evgeny V. Rebrov [a,d,**]

[a] School of Engineering, University of Warwick, Coventry CV4 7AL, UK
[b] Department of Chemistry, University of Warwick, Coventry CV4 7AL, UK
[c] School of Chemical Engineering, The University of Adelaide, Adelaide, SA 5005, Australia
[d] Department of Chemical Engineering and Chemistry, Eindhoven University of Technology, P.O. Box 513, Eindhoven 5600 MB, the Netherlands

ARTICLE INFO

Keywords:
Ir/TiO_2
Combustion-evaporation
CO_2 hydrogenation
Surface-confined plasma

ABSTRACT

The hydrogenation of CO_2 to methane over a 20 wt% Ir/TiO_2 catalytic coating has been investigated in a tubular dielectric barrier discharge (DBD) reactor. The 1.2 μm Ir/TiO_2 coating was deposited onto the inner wall of a quartz tube by a combustion-evaporation method from a mixture containing a Ti precursor and a colloidal suspension of Ir nanoparticles (2 nm). The catalyst was characterised by XRD, SEM, TEM/EDS and CO chemisorption. The Ir(0) state in the as-synthesised film was confirmed by XPS. The CH_4 conversion increased by 1.5 times, as compared to an empty tube. A maximum CO_2 conversion rate of 2.1 μmol s^{-1} was achieved at a fuel production efficiency of 3.5%. Surface reactions onto the catalyst surface are responsible for enhancement of reaction rate. The results presented in this work open up new possibilities in plasma-catalysis, whereby efficient reactions can be carried out over small volumes of catalyst.

1. Introduction

Carbon capture and utilisation (CCU) is rapidly being recognised as a key aspect of a sustainable future [1]. If appropriately harnessed, CCU technologies could enable the realisation of a circular economy, within which greenhouse gases are recycled by converting them into fuels [2]. The fundamental difficulty in activating CO_2 arises from its inertness, caused by the lack of a dipole moment in conjunction with huge thermochemical stability of the C═O bond (783 kJ mol^{-1}) [3]. CO_2 is a thermodynamic product of every organic compound which is often unused due to high process costs. Biochemical/biological, photochemical, photoelectrochemical and traditional thermal catalytic routes such as Fischer-Tropsch synthesis are commonly employed, with several advantages and disadvantages in each case. These CO_2 reduction methods are characterised by low selectivity leading to various products and therefore complicated purification procedures, low yields, and product mixtures which often require recycling at high energy cost. These processes and the materials they make use of are also often difficult to scale-up. CO_2 hydrogenation provides routes to CO and CH_4 [4–6], as well as oxygenates and higher alkanes, which can be used as fuels [7–9].

Plasma-assisted conversion of CO_2 allows a more efficient small-scale implementation. In the plasma phase, gas molecules are bombarded by electrons producing energetically excited, highly reactive gas species. Non-thermal plasma (NTP) reactors operate at ambient temperatures and pressures [10–13] and are modular and easily scalable [14] making them attractive for decentralised operation [15,16]. Ozone synthesis and decomposition of volatile organic compounds have already been implemented on industrial scale [17–19]. NTP reactors have also been used for CO_2 hydrogenation [20,21], N_2 fixation [22,23], and H_2S decomposition [24]. The reactors are powered by electricity, and so can operate using entirely renewable inputs, thus being a promising approach for storing renewable electricity as chemical energy in fuels.

Plasma produces many possible active intermediates, leading to a plethora of products, potentially requiring costly separation steps. In order to selectively convert these highly reactive intermediates into desired products, a catalytic coating can be used to direct the reaction

* Corresponding author.
** Corresponding author at: Department of Chemical Engineering and Chemistry, Eindhoven University of Technology, P.O. Box 513, Eindhoven 5600 MB, the Netherlands.
E-mail addresses: Nima.Pourali@warwick.ac.uk (N. Pourali), e.rebrov@warwick.ac.uk, e.rebrov@tue.nl (E.V. Rebrov).

https://doi.org/10.1016/j.apcata.2024.119639
Received 21 November 2023; Received in revised form 20 February 2024; Accepted 23 February 2024
Available online 24 February 2024

[10]. Maximising mass transport rates of plasma species to the catalyst surface is still a challenge [13] as the characteristic lifetime of plasma species is rather short (in the order of few microseconds to milliseconds) and they often need to travel over distances in the mm range to reach the catalyst surface [25]. This provides one of the fundamental challenges of combining plasma with catalysis and to improve existing plasma-catalytic systems, enhancing the interaction of active species with catalyst surfaces is as important as synthesising and testing new catalysts. It is also crucial to understand the extent to which the surface of the material is altering the chemistry taking place, as other factors, particularly as a change in discharge behaviour, can be the real cause of effects observed [26,27]. The combination of plasma with heterogeneous photocatalysis, involving TiO_2 as catalyst or catalyst support under UV-irradiation, is a growing field [13]. However, catalysts with tunable properties for plasma-assisted CO_2 reduction are not yet at a mature level and there are still major questions to answer about what properties enhance a material's ability to catalyse reactions in the plasma phase.

Plasma-induced vibrationally excited CO_2 must directly (despite the short lifetime of the excited species) reach the catalyst in order to be activated at a lower energy than the first dissociation step on its surface. This can be done if the catalyst forms a thin, porous layer on the inner surface of the reactor wall. For this purpose, mesoporous thin films as catalyst supports provide the shortest pathway for reactive species to reach catalytic active sites [28,29]. A commonly-used technique for film preparation is sol-gel processing. This involves depositing a complex fluid on a microstructured substrate by dip, spin, or spray coating, followed by surfactant removal to form the porous nanostructures. To facilitate the adsorption of hydrogen and/or organic species, metal nanoparticles such as Pd [30,31], Au [32], and bimetallic PtSn [33], are added to the synthesis solution. Cu and copper oxides [20,34], Ru [35] and Pd [36] are reported as active, near room temperature catalysts for CO_2 hydrogenation.

Previously we developed an elegant strategy by which a uniform coating containing controlled amounts of (poly)metallic nanoparticles can be obtained [37]. This is based on the condensation of metal oxide species by self-assembly in the presence of metallic colloids. A DBD reactor recently reported in our group uses a helical electrode which generates plasma near the catalyst surface [38]. A combination of the helical electrode with a thin catalyst layer allows the formation of plasma CO_2 species directly over the surface of the catalyst and within the pores of the support, rather than generating plasma species too far from the catalyst surface and operating in an effective post-plasma catalysis mode, as is used in many other works.

In an attempt to develop an efficient NTP catalyst for CO_2 hydrogenation, iridium is employed as an active catalyst on a titania support. It is able to dissociate hydrogen at room temperature [39] and it can also absorb hydrogen in the subsurface layer [40,41]. Supported Ir catalysts can initiate many reactions at room temperature or slightly above it. For example, a supported Ir catalyst was employed in decomposition of 1, 1-dimethyl hydrazine (unsymmetrical dimethylhydrazine, UDMH, technical name: heptyl), which is the main component of rocket fuels. Ir nanoparticles are typically added onto support in the range between 1 and 50 wt%, but for economic reasons, the lower concentrations are preferred [42]. A 32.9 wt% Ir/Al_2O_3 was employed for UDMH oxidation in a pilot plant where the main catalytic reactor operated under fluidised bed conditions [43]. Supported Ir catalysts were also used in CO_2 hydrogenation. A 20 wt% Ir/CeO_2 catalyst provided a CO_2 conversion of 8.8% at 300°C and a pressure of 1 MPa [44] while a 10 wt% Ir/In_2O_3 gave a CO_2 conversion of 17.7% at 300°C and a pressure of 5 MPa [45]. Ir/TiO_2 catalysts have not yet, however, been used for the plasma assisted hydrogenation of CO_2.

This study presents the synthesis of Ir/TiO_2 thin films onto the inner surface of a quartz tube and their catalytic performance in the plasma assisted hydrogenation of CO_2 to CH_4 in a DBD reactor with a helical electrode. The reactor used in this study is designed to maximise the interaction between the catalyst and the plasma. A discharge is generated in a small volume close to the catalyst surface to enhance efficiency and to intensify plasma-catalytic effects. It is hypothesised that this interaction enhancement will enable catalysis to take place over a thin film, without the need for greater quantities of catalyst material in the form of powder or pellets. The objective of the study was to utilise a helical electrode to generate a surface confined plasma on the catalyst surface, demonstrating the effectiveness of this novel plasma-catalyst configuration. Broadly, the target is to demonstrate the feasibility of a simple and compact reactor to hydrogenate CO_2 in an energy efficient way by initial plasma activation followed by hydrogenation on the catalyst surface.

2. Experimental

2.1. Preparation of Ir/TiO_2 thin films

Aqueous $IrCl_3$ (2.85 mM, 360 mL, 88.5 wt%, Merck) was heated to 75 °C under stirring. Ice cold aqueous $NaBH_4$ (0.1 M, 15 mL, 97 wt%, Scientific Laboratory Supplies Ltd.) was added to the $IrCl_3$ solution, and the reaction mixture was stirred for 30 min at 75°C. The reaction mixture was subsequently cooled to room temperature. Polyvinylpyrrolidone (1.0 g, MW = 10,000, Sigma-Aldrich) was added to the solution, which was then stirred for 12 h. Water was removed by heating at 70 °C and the Ir nanoparticles were redispersed in methanol (20 mL, 99.8 vol%, Sigma-Aldrich).

A catalytic film was produced on the inner surface of a quartz tube (i.d: 3 mm, o.d.: 5 mm, Robson Scientific) using a method adopted from Peeters *et al.* [46] and a coating protocol from Svetlov *et al.* [47]. A quartz tube was activated using aqueous NaOH (4 M, Honeywell) and then washed with water. PVP (3.0 g, MW = 40,000), P25 TiO_2 (0.3 g), methanol (20 mL for Ir/TiO_2 films, 40 mL for TiO_2 films), and the Ir nanoparticle suspension (20 mL) were mixed for 30 min to produce the solution. The solution was fed with a syringe pump and mixed with air flow in a T-mixer. The resulting two-phase mixture provides an annular flow with the gas core in the centre of the tube and the liquid flowing in the annulus between the gas core and the inner channel wall. Then the two-phase (air-liquid) flow enters the quartz tube from its bottom end. At the same time, the quartz tube was fed into the tubular furnace using a stepper motor at a displacement speed of 6.6 cm min^{-1}. The furnace was maintained at a temperature of 175 °C. At the exit from the oven, complete evaporation of solvent occurred, resulting in a thin solid layer attached to the inner wall of the tube. The coated tube was calcined in air for 2 h at 450 °C with a heating rate of 1 K min^{-1}, cooled to room temperature, and then reduced under a 5 vol% H_2/N_2 mixture for 2 h at 450 °C with a heating rate of 1 K min^{-1}. The coated tubes were cut to sections with a length of 250 mm. A powder was also obtained by the same method to complete characterisation, as the films provided too little material.

2.2. Characterisation of catalysts

The phase composition was determined with X-ray diffraction (XRD) using an Anton Paar XRDynamic 500 instrument equipped with Co $K\alpha_{1/2}$ radiation over the range 2θ = 20–70° at a scanning rate of 0.08 ° min^{-1}. Grazing incidence measurements were made at several different incident angles, ω. The sample height was aligned to ensure the sample surface was in the centre of rotation of the goniometer. The phases present in the coatings and the anatase/rutile ratio were determined using multi-phase Rietveld refinements, performed using the GSASII software [48]. The film thickness was measured by scanning electron microscopy (SEM) using a Zeiss SUPRA 55VP FEGSEM apparatus. Particle size was determined by transmission electron microscopy (TEM), conducted using a JEOL JEM-2100 Plus apparatus operated at 200 kV. For average particle sizes, a sample of a minimum of 100 particles was used. Energy dispersive X-ray spectroscopy (EDS) was carried out using

a JEOL ARM 200 F equipped with a 100 mm^2 EDS detector (Oxford Instruments). Nitrogen chemisorption measurements were carried out using an ASAP 2020 PLUS instrument (Micromeritics). Samples were degassed under vacuum at 30 °C for 30 min, then heated to 120 °C at a heating rate of 10 K min^{-1} and held at that temperature for 3 h under vacuum. The Ir dispersion was determined by CO chemisorption. Before measuring the CO chemisorption isotherm, the catalysts were reduced at 450 °C for 1 h (heating rate 10 K min^{-1}) and the vessel was evacuated (10 mPa) for 30 min. Desorption isotherms were measured at room temperature. The total amount of chemisorbed CO atoms was obtained by extrapolating the linear part of the isotherm to zero pressure. Correction for chemisorption on the support was not necessary, because the extrapolated values of the desorption isotherms for the titania supports, were zero within the uncertainty of the measurements. Oxidation states of surface atoms were determined by X-ray photoelectron spectroscopy (XPS) using a Kratos Axis Ultra DLD spectrometer with base pressure below 1.0 × 10^{-10} mbar. Samples were illuminated using a monochromated Al Kα X-ray source (hν = 1486.7 eV) at a take-off angle of 90 ° with respect to the surface parallel. The core level spectra were recorded using a pass energy of 20 eV (resolution ≈ 0.4 eV, step size 0.1 eV), from an analysis area of 300 ×700 μm. CasaXPS software was used to analyse the data.

2.3. Catalytic tests

A copper helix (o.d. 3.0 mm, wire thickness 0.35 mm, pitch 5.0 mm) was inserted inside the coated tubes and connected to the power supply as the high voltage electrode (Fig. 1). Aluminum foil (length: 200 mm) was attached to the outer tube surface as the ground electrode. A small opening was made in the ground electrode for OES measurements during the reaction. The electrodes were connected to a high voltage plasma generator (G2000, Redline Technologies) providing sinusoidal wave voltages with an amplitude of 5.4–6.2 kV (peak to peak) and a frequency of 68 kHz. The voltage was measured with a high voltage probe (P6015A, Tektronix). The current was measured using a Rogowski coil (6600, Pearson). A 10 nF capacitor was introduced to the ground line for monitoring the electric charges generated in the plasma. An oscilloscope (PicoScope 6000 Series, Picotech) was used to record electrical signals.

A mixture of CO_2 and H_2 was fed via the reactor with a set of mass flow controllers (Bronkhorst) at 20 °C. An optical emission spectrometer (200–900 nm, FERGIE, Princeton Instruments) fitted with an optical fibre was used for measurements of reaction intermediates. The product mixture was analysed with a gas chromatograph (GC-2010 Pro, Shimadzu) equipped with Rt-QS-BOND and SH-Molsieve 5 Å columns and TCD and FID detectors. CO and CH_4 were the only products observed in the whole range of experimental conditions studied.

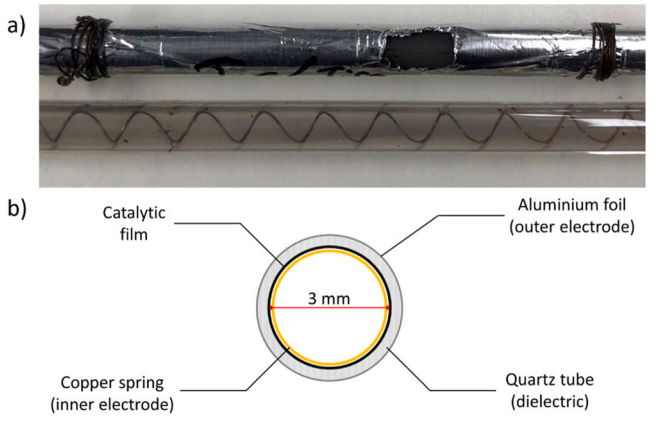

Fig. 1. (a) A photo of the Ir/TiO_2 coated tubular reactor with the ground electrode attached (top) and without the ground electrode (bottom). (b) A schematic view of the reactor cross section.

The CO_2 reaction rate and the catalytic CH_4 production rate are calculated by Eqs. (1) and (2), respectively.

$$r_{CO_2}(mol\ \ s^{-1}) = \dot{n}_{CO_2,in} - \dot{n}_{CO_2,out} \quad (1)$$

$$r_{CH_4}(mol\ \ s^{-1}\ \ g^{-1}) = \frac{\dot{n}_{CH_4,out}}{m_{cat}}, \quad (2)$$

where $\dot{n}_{CO_2,in}$ and $\dot{n}_{CO_2,out}$ are the inlet and outlet molar flow rates of CO_2 and m_{cat} is the mass of the catalyst. The CO_2 conversion and selectivity towards the two reaction products (CO and CH_4) are calculated by Eqs. (3) and (4), respectively.

$$X_{CO_2}(\%) = \frac{\dot{n}_{CO_2,in} - \dot{n}_{CO_2,out}}{\dot{n}_{CO_2,in}} \times 100, \quad (3)$$

$$S_i(\%) = \frac{\dot{n}_{i,out}}{\dot{n}_{CO_2,in} - \dot{n}_{CO_2,out}} \times 100 \quad (4)$$

and $\dot{n}_{i,out}$ is the outlet flow rate of the product. The power consumption (*P*) is calculated by integrating the product of current (*I*) and voltage (V) across the plasma gap over one period (T):

$$P(\mathrm{W}) = f\int_0^T I(t)V(t)\mathrm{d}t, \quad (5)$$

where *f* is the plasma frequency (68 kHz). Power consumption is defined here as the power dissipated in the plasma itself rather than the total amount of electrical power drawn by the system from the electrical power source. The fuel production efficiency (FPE) and energy cost (EC) were calculated by Eqs. (6) and (7) [49]:

$$FPE(\%) = \frac{LHV_{CO} \bullet \dot{n}_{CO,out} + LHV_{CH_4} \bullet \dot{n}_{CH_4,out}}{P + LHV_{H_2} \bullet \dot{n}_{H_2,in}}, \quad (6)$$

$$EC(\mathrm{Jmol}^{-1}) = \frac{P}{\dot{n}_{CO_2,in} - \dot{n}_{CO_2,out}}, \quad (7)$$

where LHV is the lower heating value of the respective gases.

3. Results and discussion

3.1. Catalyst characterisation

The XRD pattern of the Ir/TiO_2 catalyst (Fig. 2) shows a mixture of anatase and rutile phases of 90:10 (Fig. S1), a higher anatase/rutile ratio than P25 titania, alongside a broad Ir peak and minor NaCl impurity from the synthesis solution. There were no IrO_2 peaks, suggesting that the Ir was mostly Ir(0) metal.

SEM images showed the Ir/TiO_2 thin film to have a mean thickness of 1.2 μm (Fig. 3a). The as-synthesised catalyst has a high surface roughness of about 0.5 μm, but fully covers the internal surface of the quartz tube. Such morphology is good to create local mixing which enhances mass transfer of active species to the catalyst surface. In spite of the

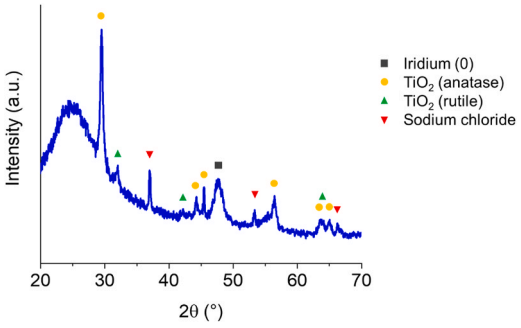

Fig. 2. XRD pattern of the Ir/TiO_2 thin film.

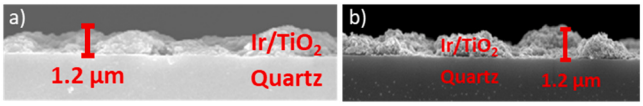

Fig. 3. SEM images of the Ir/TiO_2 thin films (a) as-synthesised and (b) spent.

differences in micron-scale morphologies, all the films are composed of very similar crystalline nanosized units. The specific surface area of the Ir/TiO_2 catalyst was 13.0 m^2g^{-1} (Fig. S2), which is a factor of 3 lower than that of P25 (50 m^2g^{-1}) [50]. The titania support demonstrates a low open porosity; the surface area was significantly lower than those of some other commercially available photocatalysts such as P25, P90, C-E100 [50]. Its low value is likely the result of coalescence of the primary particles in the combustion-evaporation process. It should be noted that vibrationally exited CO_2 species have short lifetimes (< 1 ms), and to bring them to the catalyst surface is impossible by convective mass transport. For example, a maximum lifetime of about 100 µs was estimated for vibrationally excited CO_2 [51]. Therefore, these excited species generated in the bulk gas cannot reach the outer surface of the catalyst, the only alternative is for them to be generated inside a porous catalytic structure. However, plasma can only be created in pores with dimensions larger than the Debye length, which is about 500 nm at typical plasma conditions used in this study. Such pores cannot be created by bottom-up methods and would require a different templating approach. Therefore, the support was designed to maximise the external surface area exposed to the plasma, rather than the total surface area.

To further obtain structural information for the coated films, TEM images were recorded before (Fig. 4a) and after the reaction (Fig. 4c) and the corresponding particle size distribution patterns were analysed (Fig. 4b and d, respectively). The as-synthesised Ir/TiO_2 catalyst has a rather narrow particle size distribution of Ir nanoparticles with a mean size of 2.5 nm. Similar particle size was also observed in other supported Ir catalysts used for hydrogenation [52–54]. The particles were uniformly distributed over the support although clusters can still be observed. The loading of Ir was close to the nominal loading, thus it suggests that the catalyst's composition can be controlled facilely by tuning the ratio of the precursor. A metal surface area of 4.1 $m^2\ g_{Ir}^{-1}$ was obtained from CO chemisorption experiments (Fig. S3).

A characteristic HRTEM image of the Ir/TiO_2 catalyst is shown in Fig. 5a. The Ir nanoparticles have an elongated (non-spherical) morphology. The EDS suggested that iridium was uniformly distributed across the nanoparticle while higher oxygen content was observed largely at the metal/support interface (Fig. 5b). The mean oxygen content was below 5 mol.%, which may derive from the support layer below the Ir nanoparticle.

3.2. Plasma assisted CO_2 hydrogenation

The methanation reaction requires four moles of H_2 per mole of CO_2 ($CO_2 + 4\ H_2 \rightarrow CH_4 + 2\ H_2O$). In this system, there are several points to consider. Firstly, operation at close to the stoichiometric ratio is desired, as hydrogen utilisation is important and hydrogen conversion should usually be kept close to completion to facilitate separation of reaction products. Secondly, the water gas shift (WGS) reaction between the reaction products, CO and H_2O, can take place at longer residence times and low CO_2 concentrations, therefore it is necessary to operate the reactor at short residence times and high CO_2 concentrations to eliminate the contribution from the WGS reaction to the overall reaction kinetics. Initially two H_2/CO_2 mixtures with stoichiometric (H_2 /CO_2

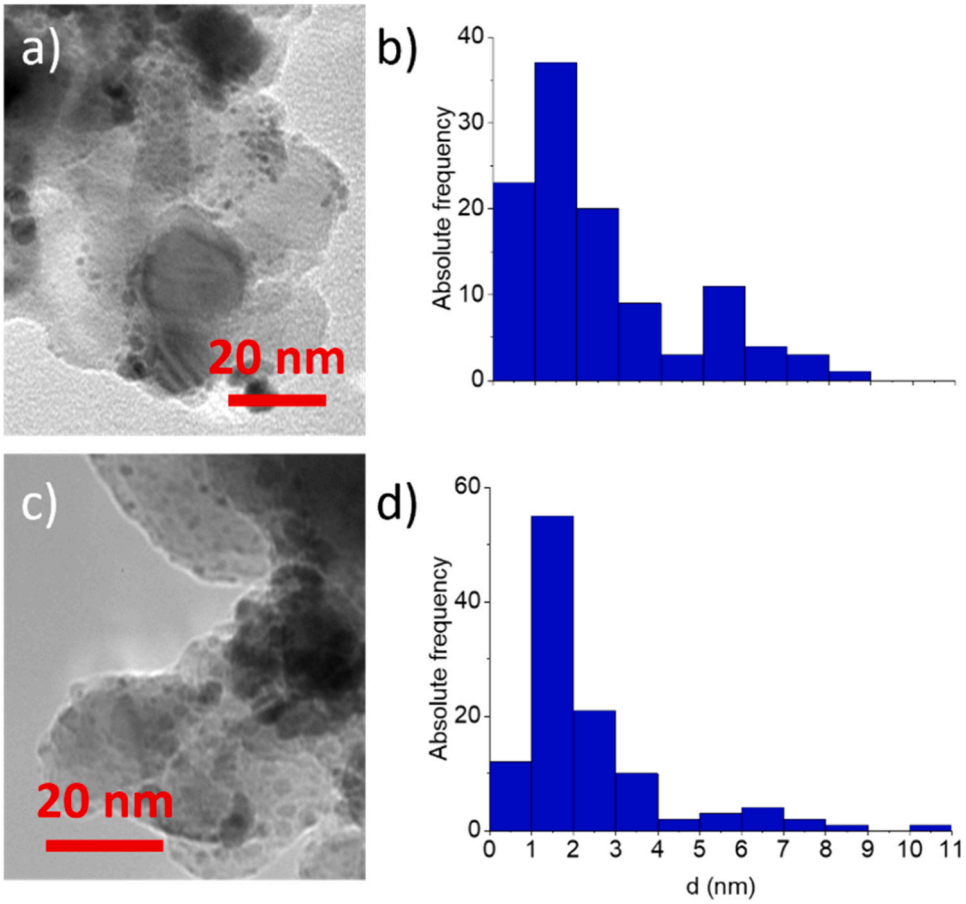

Fig. 4. TEM micrographs (a and c) and particle size distribution (b and d) of the Ir/TiO_2 thin film: as-synthesised (a and b) and spent (c and d).

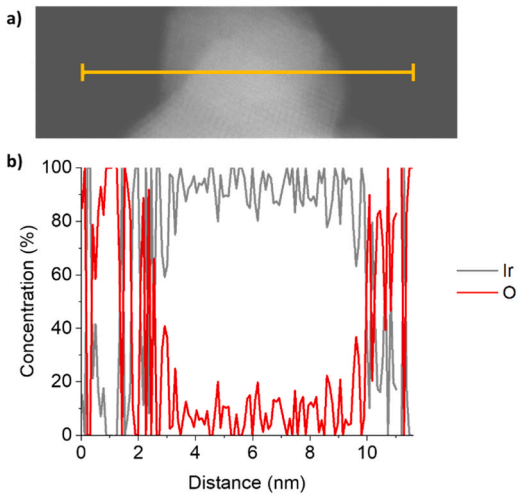

Fig. 5. (a) HRTEM micrograph of the 7 nm iridium nanoparticle from the Ir/TiO_2 catalyst. The yellow line indicates the region assessed using EDS. (b) EDS profiles for Ir and O elements.

molar ratio = 4) and substoichiometric compositions (H_2/CO_2 molar ratio = 0.5, representing large CO_2 excess) were selected for comparison of performance of uncoated, TiO_2-coated, and Ir/TiO_2-coated reactors (Fig. 6). Volumetric plasma assisted decomposition of CO_2 was observed in the empty reactor which produced CO (Fig. 6a). This rate is proportional to the plasma power, and it is influenced by the presence of the catalytic coating on the inner wall of the reactor. The deposition of a thin titania coating creates an additional dielectric layer between the two electrodes and therefore reduces the intensity of the electric field inside the reactor as well as the energy dissipation rate. The addition of a dielectric layer is known to increase energy losses in DBD reactors [10]. As a result, the amount of energy for the chemical reaction decreases, which leads to a 1.5-fold decrease in fuel production efficiency at the substoichiometric H_2/CO_2 ratio for the TiO_2 coating (Fig. 6b).

The additional dielectric layer decreased the CO_2 reaction rate; however, the titania support increased the surface reaction rate which resulted in a substantial amount of CH_4 formation, even without the addition of Ir nanoparticles (Fig. 6a). As the titania support is not able to dissociate H_2 at room temperature, it may be argued that hydrogen dissociation in plasma to produce atomic hydrogen (H) and the subsequent surface reactions onto the titania surface are responsible for the 4-fold increase of CH_4 yield over the TiO_2 coating as compared to that in the empty reactor. It was suggested by Sun *et al.* that the adsorbed HOCO and HCOO species or CO could further react with adsorbed H to produce CH_4, although the elementary steps were not provided explicitly (Scheme 1) [36]. It should be noted that the coating volume is only 0.05% of the total reactor volume (reactor volume: 1.77 cm^3, coating volume: 0.96 mm^3), therefore the active discharge volume remains essentially the same in these cases and the decrease in the CO_2 rate cannot be explained by a shorter residence time, as often observed in the reactors with pelleted catalysts. The chemical equations in Scheme 1 only include the most basic and efficient dissociation paths, they do not include the many single and multistep reaction paths that occur within a CO_2 plasma, nor any chemical and system inefficiencies, including quenching, energy recuperation, energy deposition in the molecular energy states, and higher energy reaction pathways.

The OES spectra confirmed the presence of atomic hydrogen (Hα band at 652 nm) as well as several activated C-species such as CO_2^+, CH*, CO in the 332–556 nm region, in line with previously published studies [55–58] (Fig. 7). The assignment of absorption bands is listed in Table 1. The reaction below is the dissociative excitation in plasma which causes the Hα band:

$$H\alpha \text{ excitation: } e^- + H_2 \rightarrow H + H^* + e^- \ (12.1\ eV) \quad (8)$$

Once excited, the hydrogen atom releases the energy in the form of a photon and returns to the ground state.

$$H\alpha \text{ emission: } H^* \rightarrow H + h\nu \ (656\ nm) \quad (9)$$

The presence of atomic hydrogen showed that hydrogen dissociation takes place under plasma conditions. The amount of atomic hydrogen (proportional to the area of the Hα band) increases with the concentration of molecular hydrogen in the feed, while the intensity of the CO_2^+, CH, and CO peaks decrease relative to the Hα band.

The existence of an additional surface route over the TiO_2 coatings is also supported by a higher overall CO formation rate and a much higher CH_4 production rate that are due to the surface reactions in the experiment at higher CO_2 concentration in plasma (Fig. 6a). The surface rate is proportional to the number of titania active sites on the surface

$$CO_{2,ad} \longrightarrow OCO_{ad}$$

$$OCO_{ad} + H_{ad} \longrightarrow HOCO_{ad}$$

$$H_{ads} + HOCO_{ad} \longrightarrow CO_{ad} + H_2O$$

$$CO_{ad} + H_{ad} \longrightarrow CH_{ad} + OH_{ad} \longrightarrow CH_{2,ad} \longrightarrow CH_{3,ad} \longrightarrow CH_4$$

Scheme 1. Possible surface routes towards CO and CH_4. Adopted from Sun *et al.* [36].

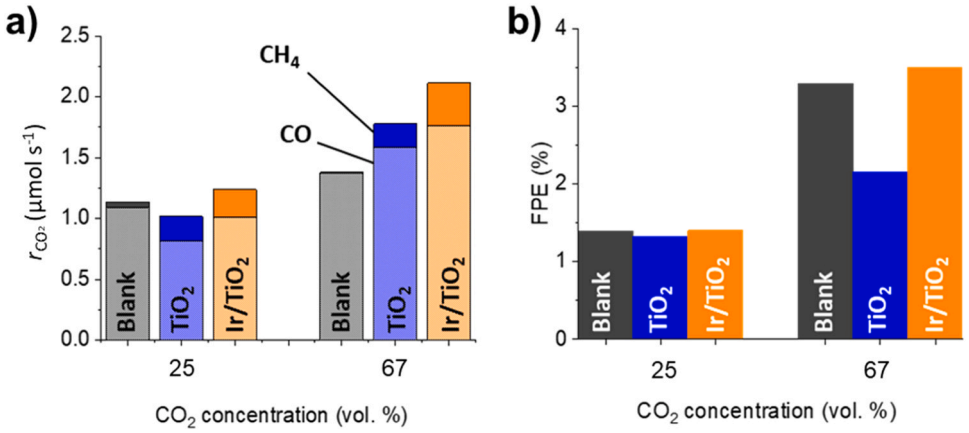

Fig. 6. (a) CO_2 reaction rate and product (CH_4 and CO) production rates, (b) fuel production efficiency (FPE) with two CO_2/H_2 mixtures containing 25 and 67 vol% CO_2 in the empty reactor (blank), over TiO_2, and over Ir/TiO_2. Voltage: 5.6 kV peak to peak.

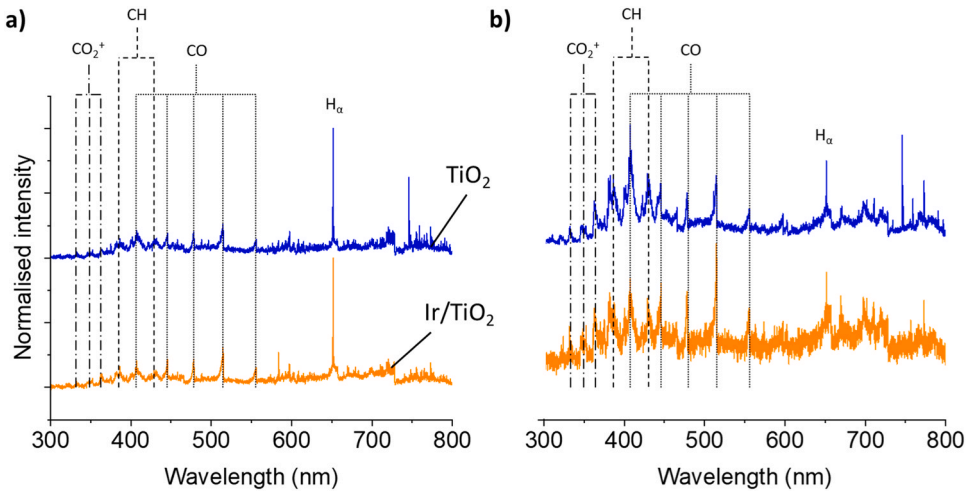

Fig. 7. Optical emission spectra of CO_2/H_2 gas mixture in the presence of TiO_2 and Ir/TiO_2 at (a) 50 vol% CO_2 and (b) 83 vol% CO_2.

Table 1
Emission lines from the OES of CO_2/H_2 gas mixture.

Species	Transition	$\Delta\vartheta$	Wavelength (nm)
CO_2^+	$A^2\Pi\ X^2\Pi$	-	332
CO_2^+	$A^2\Pi\ X^2\Pi$	-	349
CO_2^+	$A^2\Pi\ X^2\Pi$	-	362
CH(B-X)	$B^2\Sigma\ X^2\Pi$	0	386
CH(A-X)	$A^2\Sigma\ X^2\Pi$	0	429
CO	Ångström band	-1	407
CO	Ångström band	0	446
CO	Ångström band	1	478
CO	Ångström band	2	515
CO	Ångström band	3	556
$H\alpha$	Balmer n = 3	-	656

available for catalysis rather than gas phase concentration of H_2. The rate of volumetric CO_2 decomposition increases at higher CO_2 concentrations, as can be seen in Fig. 6a, as the volumetric reaction has a positive reaction order with respect to CO_2, therefore its rate is proportional to the CO_2 concentration in the reaction mixture.

Comparing the data over the Ir/TiO_2 catalyst and the TiO_2 support (Fig. 6) it can be seen that the CH_4 formation rate over the Ir/TiO_2 catalyst is faster than it is over TiO_2. This can be explained by an additional surface route for CH_4 formation over the Ir nanoparticles. The gain is more clearly pronounced in the CO_2 rich mixture (at a lower hydrogen concentration) where the contribution from the volumetric reaction to the total methane production rate decreases. In this additional route, H_2 dissociation over Ir nanoparticles plays a crucial role in promoting the additional catalytic hydrogenation steps. This catalytic route does not consume energy needed for H_2 dissociation which could explain higher energy efficiency over the Ir/TiO_2 catalyst compared to over TiO_2 (Fig. 6b).

In the next series of experiments, the effect of residence time on CO_2 reaction rate, selectivity and FPE was studied by keeping the same CO_2 flow rate while increasing the total flow rate (Fig. 8). It should be noted that the specific energy input reduces at shorter residence times and therefore it decreases the rates of volumetric plasma reactions. In line with this trend, the CO_2 reaction rate monotonously decreases from 1.1 to 0.85 μmol s^{-1} over TiO_2 as residence time decreases, while the methane selectivity increases due to a reduced contribution from the volumetric reactions leading to CO formation (Fig. 8a). In the absence of external mass transfer limitations, the rate of surface reactions does not depend on the flow rate (or residence time). However, this is clearly not the case here. The flow rate has a major influence on the reaction rate demonstrating severe mass transfer limitations and hence it is a clear

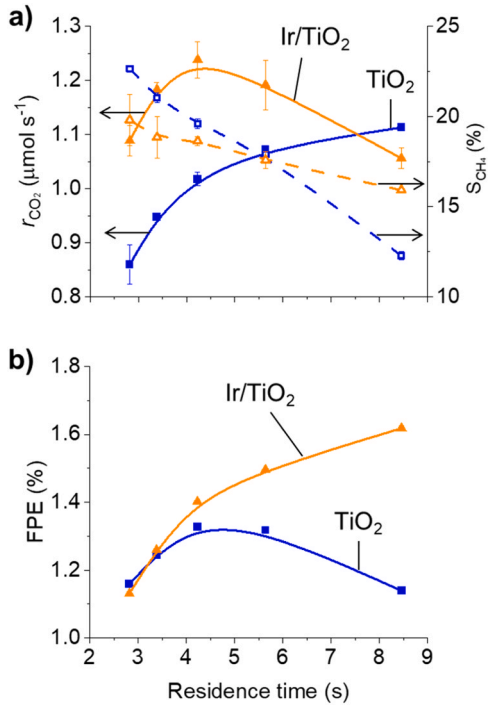

Fig. 8. (a) CO_2 reaction rate and CH_4 selectivity and (b) fuel production efficiency as a function of residence time over TiO_2 and Ir/TiO_2. CO_2 flow rate: 5 mL min^{-1}, voltage: 5.6 kV peak to peak. Lines are drawn as a guide for the eye.

disadvantage of the plasma-catalytic approach in the present configuration. In other words, the active H species cannot reach the catalyst surface before they converted to other product (water) in gas phase reactions.

The fuel production efficiency decreases at shorter residence times (Fig. 8b). This trend is observed both over Ir/TiO_2 and TiO_2. However, at longer residence time, the FPE over the support also decreases, which can be explained by heat losses due to gas heating as the active species cannot be effectively converted to CH_4 over the TiO_2 support. This fact suggests an essential role of catalytic surface reactions that take place on the Ir/TiO_2 catalyst.

Fig. 9 shows the Ir 4 f XPS spectra of the as-synthesised and spent Ir/TiO_2 catalysts. The as-synthesised catalyst was found to have exclusively Ir(0) at the surface (Table 3). From the evolution of the XPS spectra,

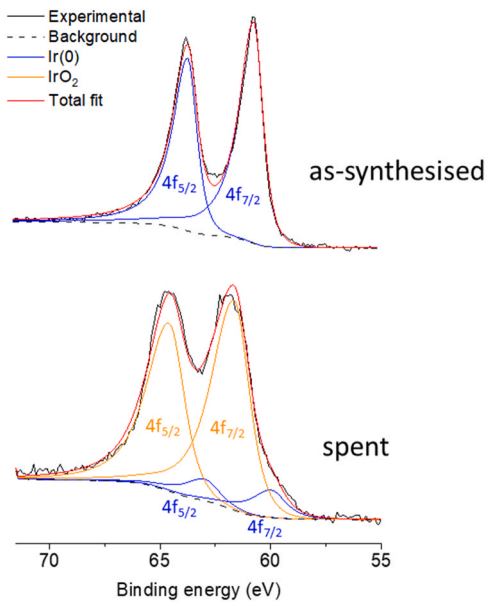

Fig. 9. Ir 4 f XPS spectra of Ir/TiO_2 coatings (a) as-synthesised, and (b) spent.

Table 2
The CO production rate over TiO_2 and Ir/TiO_2. Total flow rate: 30 mL min^{-1}, voltage: 5.6 kV peak to peak.

CO_2 concentration (vol%)	Catalytic CO production rate (μmol s^{-1})	
	TiO_2	Ir/TiO_2
67	1.6	1.8
100	2.8	1.7

there is a clear shift in the centre of gravity for the Ir 4 f core level to higher binding energies which is indicative of an overall higher oxidation state than the initial state, based on the general understanding of binding energy shift. To obtain a quantitative description of the catalyst surface after a stability test, the Ir 4 f spectra were studied using the fit models of metallic Ir and amorphous IrO_x [59,60]. The deconvolution of Ir 4 f spectra confirms a common phase, labelled as Ir, which was detected on the surface of both as-synthesised and spent Ir/TiO_2 catalysts. The only peaks fitted were the 4 $f_{7/2}$ and 4 $f_{5/2}$ associated with Ir (0) at 60.7 and 63.6 eV (corresponding with previous studies [61]). The Ir 4 f spectrum of the spent catalyst can be deconvoluted to Ir(IV), and Ir (0) with its Ir 4 $f_{7/2}$ and Ir 4 $f_{5/2}$ main peaks located at binding energies of 63.0 and 66.0 eV, respectively. In the spent catalyst, the Ir 4 $f_{7/2}$ and 4 $f_{5/2}$ bands were observed at 61.7 and 64.6 eV, respectively, suggesting that Ir(IV) [61] were the dominant form accounting for approximately 88% to the total peak area. A small fraction of Ir (0) was also observed in the spent catalyst. However, the reaction rate remains essentially the same after a time of stream of 3 h which may be due to the fact that IrO_2 is an active catalytic component and is responsible for the high selectivity observed towards CH_4. Previous studies have reported that the dehydration of hydrous Ir oxide/hydroxide, either *in-situ* in a TEM [62] or by using a high calcination temperature [63], results in an increased oxidation state of Ir. The mean particle size of the spent Ir/TiO_2 catalyst (2.3 nm) was close to that of the as-synthesised catalyst (Fig. 4a and c) and there were no changes in the morphology of the support despite the oxidation of Ir metal under the reaction conditions.

In the next series of experiments, the effect of CO_2/H_2 ratio on CO_2 reaction rate, selectivity, and energy efficiency was studied at a fixed residence time. Activation energy is the minimum input energy needed to start a reaction. The activation energy for CO_2 dissociation is 532 kJ mol^{-1} (5.52 eV).

$$CO_2 + \text{heat} \rightarrow CO + O \quad (10)$$

Fig. 10a shows that the CO_2 reaction rate increases almost linearly with an increase in CO_2 concentration at a fixed flow rate over both TiO_2 and Ir/TiO_2. This result, alongside increasing CO selectivity with increasing CO_2 concentration, suggests that volumetric CO_2 dissociation is playing a substantial role in the overall reactivity. However, at the highest CO_2 concentration, the reaction rate over the Ir/TiO_2 catalyst slightly decreases and the absolute value becomes less than that over TiO_2. This can be explained by the presence of an additional pathway which consumes CO to produce CO_2 over Ir nanoparticles as this effect was not observed over TiO_2. It can be assumed that CO_2 dissociation produces a large amount of oxygen which cannot be fully consumed in the reaction with hydrogen at high CO_2 concentrations. This oxygen can be adsorbed onto Ir nanoparticles and contribute to CO oxidation, which can take place at room temperature over Ir nanoparticles [64]. In the study which demonstrated this, it was proposed that the CO reaction order changes from negative to positive as the CO partial pressure increases. According to this line of reason, the CO oxidation reaction rate would not contribute noticeably to the overall reaction at low CO concentrations in the gas mixture, which is concurrent with the experimental observations. Moreover, oxygen is fully consumed in the reaction with atomic hydrogen to produce water at lower CO_2 concentrations. Increasing the CO_2 concentration to 100% resulted in a much higher CO production rate over the TiO_2 support as compared to that over Ir/TiO_2 catalyst (Table 2), which would be expected if Ir were to catalyse the oxidation of CO back to CO_2. The results highlight that there exists an optimum CO_2 concentration which provides the highest reaction rate in the plasma assisted catalysis of CO_2 hydrogenation.

Fig. 10b shows that FPE monotonously increases with the CO_2 concentration over both TiO_2 and Ir/TiO_2. The ionisation of H_2 requires more energy than that of CO_2, meaning that at the lower CO_2 concentration, reaction rate and FPE are greater. By changing the CO_2 concentration from 17 to 83 vol%, FPE was enhanced by a factor of 3, which can be partly ascribed to the reduced energy losses for H_2 excitation, with H_2 activation possible on the surface of Ir nanoparticles.

The CO_2 conversion increased with plasma power at low (17%) and

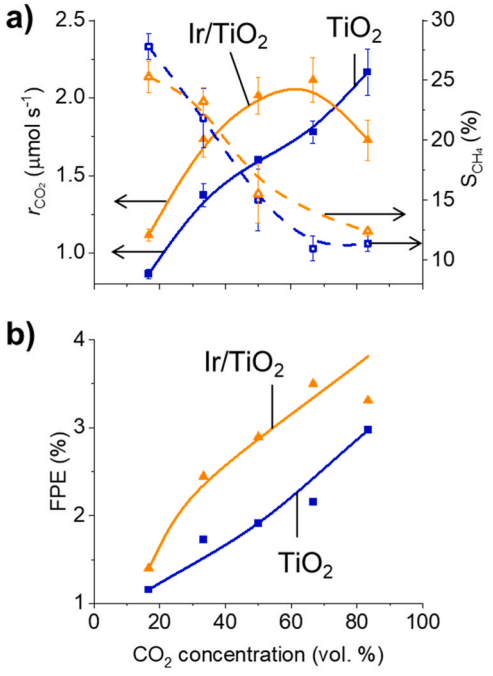

Fig. 10. (a) CO_2 conversion rate and CH_4 selectivity and (b) fuel production efficiency with varying CO_2 concentration over TiO_2 and Ir/TiO_2. Total flow rate: 30 mL min^{-1}, voltage: 5.6 kV peak to peak. Lines are drawn as a guide for the eye.

Table 3
Binding energies and bonding environment assignments of the peaks observed in the Ir 4 f region of the XPS of the as-synthesised and spent Ir/TiO_2 catalysts.

Catalyst	Binding energy (eV)	Peak area (%)	Bonding environment
As-synthesised	60.7	50.1	Ir 4 $f_{7/2}$ – Ir(0)
	63.6	49.9	Ir 4 $f_{5/2}$ – Ir(0)
Spent	60.0	5.9	Ir 4 $f_{7/2}$ – Ir(0)
	63.0	5.9	Ir 4 $f_{5/2}$ – Ir(0)
	61.7	43.7	Ir 4 $f_{7/2}$ – IrO_2
	64.6	44.6	Ir 4 $f_{5/2}$ – IrO_2

high (83%) CO_2 concentration (Fig. 11a), in line with other literature studies. The power did not appear to affect the selectivity either; the selectivity lines were almost horizontal in the entire range of applied power. Fig. 11b shows that FPE decreased with increasing power at a CO_2 concentration of 83% but did not change at a CO_2 concentration of 17%. These data are in line with those in Fig. 10b, where increasing the CO_2 concentration significantly enhances FPE.

The CO_2 conversion in the plasma assisted hydrogenation reaction at optimised conditions was higher than that reported by most other researchers (Fig. 12a). While the main reaction product was CO, the catalytic rate of methane formation was two orders of magnitude higher than most other studies (Fig. 12b). This can be somewhat attributed to the use of thin catalytic films rather than pellets in this study, meaning that the catalyst mass is generally orders of magnitude smaller than those used in other work. The CO_2 ionisation energy is shown with a dashed line. A thermal-catalytic process with energy costs lower than this is also shown for comparison.

4. Conclusions

1.2 μm thick Ir/TiO_2 thin films were deposited onto the inner surface of a DBD tubular reactor. The CO_2 conversion in the plasma assisted hydrogenation reaction at optimised conditions was higher than that reported in other studies at the same level of energy efficiency. Methane production was enhanced in plasma assisted CO_2 hydrogenation over the Ir/TiO_2 catalysts compared to the reaction without a catalyst. Hydrogen dissociation was observed under plasma conditions. The Ir nanoparticles were oxidised in the course of the reaction, however the particle size and dispersion remained essentially the same in spent catalysts. The amount of atomic hydrogen in plasma increased with the concentration of molecular hydrogen in the feed, at the same time the energy efficiency decreased. Increasing the H_2 concentration in the feed was hypothesised to saturate active sites, meaning that the rate of CO_2 hydrogenation decreased after an optimum H_2 concentration. An optimum in fuel production efficiency was found in a CO_2/H_2 mixture containing 60 vol% CO_2.

The design of the reactor provides a proof-of-concept that the interaction of plasma-generated species with the catalytic film can be maximised, leading to noticeable changes in the chemistry observed. In this case, the effect of the catalyst can be clearly distinguished from any other effects, as the selectivity was altered so drastically. It was not simply a case of conversion or efficiency enhancement, which can result from the improvement of electrical properties, but the accessing of a reaction pathway to produce methane at rates favourable when compared with other literature values, which contributes negligibly to the chemistry observed when no catalyst was present. This was achieved using a small quantity of catalytic material, demonstrating that reactor design, utilising a helical electrode to generate plasma species on the catalyst surface, enhanced plasma-catalyst interactions. Such design improvements are crucial to efforts in research towards improving plasma-catalytic systems for reaction selectivity towards high-value products.

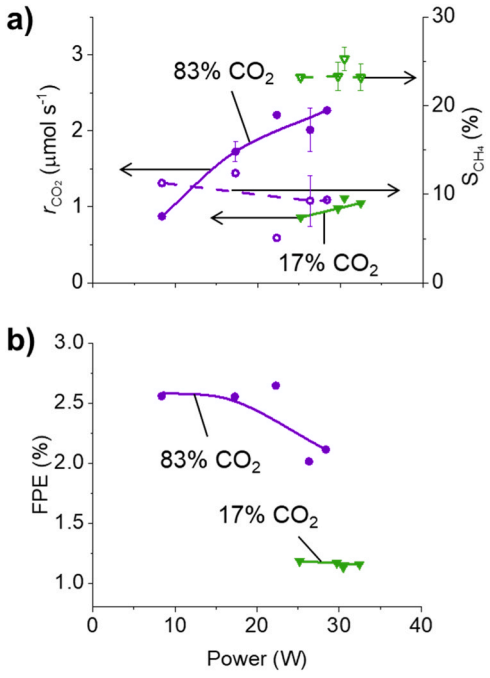

Fig. 11. (a) CO_2 reaction rate and CH_4 selectivity, (b) FPE as a function of plasma power over TiO_2 thin films. The power was varied by setting different voltages. Total flow rate: 30 mL min^{-1}, voltage: 5.6 kV. Lines are drawn as a guide for the eye.

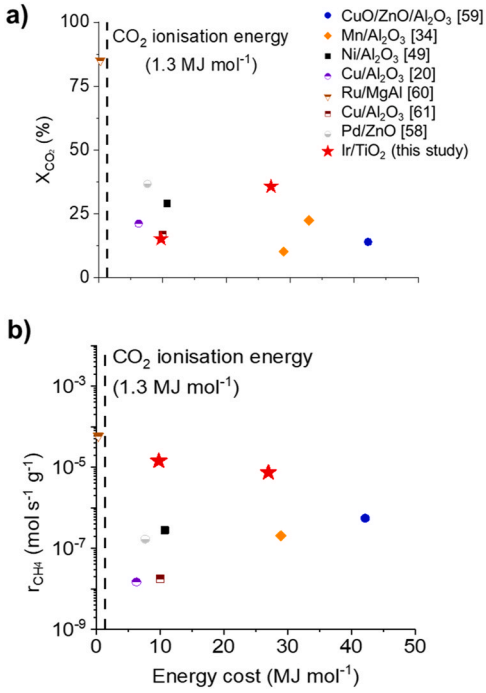

Fig. 12. A comparison of the values obtained in this study with data from other reported plasma CO_2 hydrogenation studies comparing energy cost with (a) conversion (b) production rate of CH_4 [20,34–36,49,65,66].

CRediT authorship contribution statement

Volker Hessel: Writing – review & editing, Supervision. **Richard Walton:** Writing – review & editing, Supervision. **Yuyan Gong:** Writing – original draft, Investigation. **Nima Pourali:** Writing – review & editing, Methodology, Investigation, Formal analysis, Conceptualization. **Joseph Gregory:** Writing – original draft, Investigation. **Evgeny Rebrov:** Writing – review & editing, Supervision, Funding acquisition,

Formal analysis, Data curation, Conceptualization.

Declaration of Competing Interest

The authors declare that they have no known competing financial interests or personal relationships that could have appeared to influence the work reported in this paper

Data availability

Data will be made available on request.

Acknowledgements

The authors acknowledge funding from the European Research Council (ERC) under the European Union's Horizon 2020 research and innovation program (grant agreement No 810182); ERC Synergy Grant SCOPE, "Surface-COnfined fast-modulated Plasma for process and Energy intensification in small molecules conversion". The authors also acknowledge the support from Electron Microscopy Research Technology Platform and XRD Research Technology Platform and Dr David Walker, Jacob Oyarzabal and Mark Crossman for their help with XRD measurements and interpretation. We thank Dr. Marc Walker and Katie S. Pickering for their help with XPS and N_2 adsorption experiments, respectively. We thank Prof. Salvatore Abate from the University of Messina for CO chemisorption measurements. We thank Steven Mollart for his help with producing the graphical abstract. We thank Johnson Matthey for loan of the iridium salt under their PGM Award Scheme.

References

[1] R.M. Cuéllar-Franca, A. Azapagic, Carbon capture, storage and utilisation technologies: A critical analysis and comparison of their life cycle environmental impacts, J. CO2 Util. 9 (2015) 82–102, https://doi.org/10.1016/j.jcou.2014.12.001.

[2] M. Geissdoerfer, P. Savaget, N.M.P. Bocken, E.J. Hultink, The Circular Economy – A new sustainability paradigm? J. Clean. Prod. 143 (2017) 757–768, https://doi.org/10.1016/j.jclepro.2016.12.048.

[3] R. Snoeckx, A. Bogaerts, Plasma technology-a novel solution for CO2 conversion? Chem. Soc. Rev. 46 (2017) 5805–5863, https://doi.org/10.1039/c6cs00066e.

[4] I. Graça, L.V. González, M.C. Bacariza, A. Fernandes, C. Henriques, J.M. Lopes, M. F. Ribeiro, CO2 hydrogenation into CH4 on NiHNaUSY zeolites, Appl. Catal. B Environ. 147 (2014) 101–110, https://doi.org/10.1016/j.apcatb.2013.08.010.

[5] S. Kattel, P. Liu, J.G. Chen, Tuning Selectivity of CO2 Hydrogenation Reactions at the Metal/Oxide Interface, J. Am. Chem. Soc. 139 (2017) 9739–9754, https://doi.org/10.1021/jacs.7b05362.

[6] C. Yang, S. Liu, Y. Wang, J. Song, G. Wang, S. Wang, Z.J. Zhao, R. Mu, J. Gong, The Interplay between Structure and Product Selectivity of CO2 Hydrogenation, Angew. Chem. - Int. Ed. 58 (2019) 11242–11247, https://doi.org/10.1002/anie.201904649.

[7] R.P. Ye, J. Ding, W. Gong, M.D. Argyle, Q. Zhong, Y. Wang, C.K. Russell, Z. Xu, A. G. Russell, Q. Li, M. Fan, Y.G. Yao, CO2 hydrogenation to high-value products via heterogeneous catalysis, Nat. Commun. 10 (2019), https://doi.org/10.1038/s41467-019-13638-9.

[8] P. Gao, L. Zhang, S. Li, Z. Zhou, Y. Sun, Novel heterogeneous catalysts for CO2 hydrogenation to liquid fuels, ACS Cent. Sci. 6 (2020) 1657–1670, https://doi.org/10.1021/acscentsci.0c00976.

[9] S. Saeidi, S. Najari, V. Hessel, K. Wilson, F.J. Keil, P. Concepción, S.L. Suib, A. E. Rodrigues, Recent advances in CO2 hydrogenation to value-added products — Current challenges and future directions, Prog. Energy Combust. Sci. 85 (2021) 100905, https://doi.org/10.1016/j.pecs.2021.100905.

[10] R.S. Abiev, D.A. Sladkovskiy, K.V. Semikin, D.Y. Murzin, E.V. Rebrov, Non-thermal plasma for process and energy intensification in dry reforming of methane, Catalysts 10 (2020) 1–41, https://doi.org/10.3390/catal10111358.

[11] N. Pourali, M.M. Sarafraz, V. Hessel, E.V. Rebrov, Simulation study of a pulsed DBD with an electrode containing charge injector parts, Phys. Plasmas 28 (2021), https://doi.org/10.1063/5.0027562.

[12] P. Chawdhury, D. Ray, T. Vinodkumar, C. Subrahmanyam, Catalytic DBD plasma approach for methane partial oxidation to methanol under ambient conditions, Catal. Today 337 (2019) 117–125, https://doi.org/10.1016/j.cattod.2019.03.032.

[13] C.A. Aggelopoulos, Recent advances of cold plasma technology for water and soil remediation: A critical review, Chem. Eng. J. 428 (2022) 131657, https://doi.org/10.1016/j.cej.2021.131657.

[14] Z. Jianli, Z. Juncheng, S. Ji, G. Hongchen, W. Xiangsheng, G. Weimin, Scale-up synthesis of hydrogen peroxide from H2/O2 with multiple parallel DBD tubes, Plasma Sci. Technol. 11 (2009) 181–186, https://doi.org/10.1088/1009-0630/11/2/10.

[15] A. George, B. Shen, M. Craven, Y. Wang, D. Kang, C. Wu, X. Tu, A Review of Non-Thermal Plasma Technology: A novel solution for CO2 conversion and utilization, Renew. Sustain. Energy Rev. 135 (2021) 109702, https://doi.org/10.1016/j.rser.2020.109702.

[16] D. Zhou, R. Zhou, R. Zhou, B. Liu, T. Zhang, Y. Xian, P.J. Cullen, X. Lu, K. (Ken Ostrikov, Sustainable ammonia production by non-thermal plasmas: Status, mechanisms, and opportunities, Chem. Eng. J. 421 (2021) 129544, https://doi.org/10.1016/j.cej.2021.129544.

[17] A.M. Vandenbroucke, R. Morent, N. De Geyter, C. Leys, Non-thermal plasmas for non-catalytic and catalytic VOC abatement, J. Hazard. Mater. 195 (2011) 30–54, https://doi.org/10.1016/j.jhazmat.2011.08.060.

[18] S. Li, X. Dang, X. Yu, G. Abbas, Q. Zhang, L. Cao, The application of dielectric barrier discharge non-thermal plasma in VOCs abatement: A review, Chem. Eng. J. 388 (2020) 124275, https://doi.org/10.1016/j.cej.2020.124275.

[19] M. Qu, Z. Cheng, Z. Sun, D. Chen, J. Yu, J. Chen, Non-thermal plasma coupled with catalysis for VOCs abatement: A review, Process Saf. Environ. Prot. 153 (2021) 139–158, https://doi.org/10.1016/j.psep.2021.06.028.

[20] L. Wang, Y. Yi, H. Guo, X. Tu, Atmospheric Pressure and Room Temperature Synthesis of Methanol through Plasma-Catalytic Hydrogenation of CO2, ACS Catal. 8 (2018) 90–100, https://doi.org/10.1021/acscatal.7b02733.

[21] S. Li, E. Rebrov, F. Gallucci, V. Hessel, CO2 Hydrogenation With a Dielectric Barrier Discharge Reactor, Chem. Valoris. Carbon Dioxide, : Green. Chem. Ser. (2022) 446–465.

[22] A. Bogaerts, E.C. Neyts, Plasma Technology: An Emerging Technology for Energy Storage, ACS Energy Lett. 3 (2018) 1013–1027, https://doi.org/10.1021/acsenergylett.8b00184.

[23] P. Lamichhane, N. Pourali, E.V. Rebrov, V. Hessel, Energy Intensified Nitrogen Fixation Through Fast Modulated Gas Discharge from Pyramid-shaped Micro-electrode, Plasma Chem. Plasma Process. (2023), https://doi.org/10.1007/s11090-023-10376-1.

[24] E. Linga Reddy, V.M. Biju, C. Subrahmanyam, Production of hydrogen and sulfur from hydrogen sulfide assisted by nonthermal plasma, Appl. Energy 95 (2012) 87–92, https://doi.org/10.1016/j.apenergy.2012.02.010.

[25] A. Bogaerts, G. Centi, V. Hessel, E. Rebrov, Challenges in unconventional catalysis, Catal. Today 420 (2023) 114180, https://doi.org/10.1016/j.cattod.2023.114180.

[26] X. Tu, H.J. Gallon, M.V. Twigg, P.A. Gorry, J.C. Whitehead, Dry reforming of methane over a Ni/Al2O3 catalyst in a coaxial dielectric barrier discharge reactor, J. Phys. D. Appl. Phys. 44 (2011), https://doi.org/10.1088/0022-3727/44/27/274007.

[27] F.A. Herrera, G.H. Brown, P. Barboun, N. Turan, P. Mehta, W.F. Schneider, J. C. Hicks, D.B. Go, The impact of transition metal catalysts on macroscopic dielectric barrier discharge (DBD) characteristics in an ammonia synthesis plasma catalysis reactor, J. Phys. D. Appl. Phys. 52 (2019), https://doi.org/10.1088/1361-6463/ab0c58.

[28] O. Muraza, E.V. Rebrov, T. Khimyak, B.F.G. Johnson, P.J. Kooyman, U. Lafont, M. H.J.M. de Croon, J.C. Schouten, Mesoporous silica films as catalyst support for microstructured reactors: Preparation and characterization, Chem. Eng. J. 135 (2008) 99–103, https://doi.org/10.1016/j.cej.2007.07.023.

[29] T.S. Glazneva, E.V. Rebrov, J.C. Schouten, E.A. Paukshtis, Z.R. Ismagilov, Synthesis and characterization of mesoporous silica thin films as a catalyst support on a titanium substrate, Thin Solid Films 515 (2007) 6391–6394, https://doi.org/10.1016/j.tsf.2006.11.058.

[30] N. Cherkasov, A.O. Ibhadon, E.V. Rebrov, Novel synthesis of thick wall coatings of titania supported Bi poisoned Pd catalysts and application in selective hydrogenation of acetylene alcohols in capillary microreactors, Lab Chip 15 (2015) 1952–1960, https://doi.org/10.1039/c4lc01066c.

[31] N. Cherkasov, A.O. Ibhadon, E.V. Rebrov, Solvent-free semihydrogenation of acetylene alcohols in a capillary reactor coated with a Pd-Bi/TiO2 catalyst, Appl. Catal. A Gen. 515 (2016) 108–115, https://doi.org/10.1016/j.apcata.2016.01.019.

[32] E.V. Rebrov, A. Berenguer-Murcia, B.F.G. Johnson, J.C. Schouten, Gold supported on mesoporous titania thin films for application in microstructured reactors in low-temperature water-gas shift reaction, Catal. Today 138 (2008) 210–215, https://doi.org/10.1016/j.cattod.2008.06.029.

[33] Z.R. Ismagilov, E.V. Matus, A.M. Yakutova, L.N. Protasova, I.Z. Ismagilov, M. A. Kerzhentsev, E.V. Rebrov, J.C. Schouten, Design of Pt-Sn catalysts on mesoporous titania films for microreactor application, Catal. Today 147 (2009) 81–86, https://doi.org/10.1016/j.cattod.2009.07.046.

[34] Y. Zeng, X. Tu, Plasma-Catalytic CO2 Hydrogenation at Low Temperatures, IEEE Trans. Plasma Sci. 44 (2016) 405–411, https://doi.org/10.1109/TPS.2015.2504549.

[35] S. Xu, S. Chansai, Y. Shao, S. Xu, Y. chi Wang, S. Haigh, Y. Mu, Y. Jiao, C.E. Stere, H. Chen, X. Fan, C. Hardacre, Mechanistic study of non-thermal plasma assisted CO2 hydrogenation over Ru supported on MgAl layered double hydroxide, Appl. Catal. B Environ. 268 (2020) 118752, https://doi.org/10.1016/j.apcatb.2020.118752.

[36] Y. Sun, J. Wu, Y. Wang, J. Li, N. Wang, J. Harding, S. Mo, L. Chen, P. Chen, M. Fu, D. Ye, J. Huang, X. Tu, Plasma-Catalytic CO2Hydrogenation over a Pd/ZnO Catalyst: In Situ Probing of Gas-Phase and Surface Reactions, JACS Au 2 (2022) 1800–1810, https://doi.org/10.1021/jacsau.2c00028.

[37] E. Rebrov, A. Berenguer-Murcia, A. Wheatley, B. Johnson, J. Schouten, Thin catalytic coatings on microreactor walls: a way to make industrial processes more efficient, Chim. Oggi 27 (2009) 4–7.

[38] N. Pourali, K. Lai, J. Gregory, Y. Gong, V. Hessel, E.V. Rebrov, Study of plasma parameters and gas heating in the voltage range of nondischarge to full-discharge in a methane-fed dielectric barrier discharge, Plasma Process. Polym. 20 (2023), https://doi.org/10.1002/ppap.202200086.

[39] G.B. McVicker, R.T.K. Baker, R.L. Garten, E.L. Kugler, Chemisorption properties of iridium on alumina catalysts, J. Catal. 65 (1980) 207–220, https://doi.org/10.1016/0021-9517(80)90295-X.
[40] T.S. Marinova, D.V. Chakarov, Coadsorption of carbon monoxide and hydrogen on iridium single crystals, Surf. Sci. 217 (1989) 65–77, https://doi.org/10.1016/0039-6028(89)90535-9.
[41] H. Kobayashi, M. Yamauchi, H. Kitagawa, Finding hydrogen-storage capability in iridium induced by the nanosize effect, J. Am. Chem. Soc. 134 (2012) 6893–6895, https://doi.org/10.1021/ja302021d.
[42] J.G.E. Cohn, Catalytic Decomposition of 1,1-Dimethylhydrazine, 1963. ⟨https://patentimages.storage.googleapis.com/79/e0/7b/39edd677ce497f/US2602769.pdf⟩.
[43] Z.R. Ismagilov, M.A. Kerzhentsev, I.Z. Ismagilov, V.A. Sazonov, V.N. Parmon, G. L. Elizarova, O.P. Pestunova, V.A. Shandakov, Y.L. Zuev, V.N. Eryomin, N. V. Pestereva, F. Garin, H.J. Veringa, Oxidation of unsymmetrical dimethylhydrazine over heterogeneous catalysts: Solution of environmental problems of production, storage and disposal of highly toxic rocket fuels, Catal. Today 75 (2002) 277–285, https://doi.org/10.1016/S0920-5861(02)00080-9.
[44] S. Li, Y. Xu, Y. Chen, W. Li, L. Lin, M. Li, Y. Deng, X. Wang, B. Ge, C. Yang, S. Yao, J. Xie, Y. Li, X. Liu, D. Ma, Tuning the Selectivity of Catalytic Carbon Dioxide Hydrogenation over Iridium/Cerium Oxide Catalysts with a Strong Metal-Support Interaction, Angew. Chem. 129 (2017) 10901–10905, https://doi.org/10.1002/ange.201705002.
[45] C. Shen, K. Sun, Z. Zhang, N. Rui, X. Jia, D. Mei, C.J. Liu, Highly Active Ir/In2O3Catalysts for Selective Hydrogenation of CO2to Methanol: Experimental and Theoretical Studies, ACS Catal. 11 (2021) 4036–4046, https://doi.org/10.1021/acscatal.0c05628.
[46] H. Peeters, M. Keulemans, G. Nuyts, F. Vanmeert, C. Li, M. Minjauw, C. Detavernier, S. Bals, S. Lenaerts, S.W. Verbruggen, Plasmonic gold-embedded TiO2 thin films as photocatalytic self-cleaning coatings, Appl. Catal. B Environ. 267 (2020), https://doi.org/10.1016/j.apcatb.2020.118654.
[47] S.D. Svetlov, D.A. Sladkovskiy, K.V. Semikin, A.V. Utemov, R.S. Abiev, E. V. Rebrov, Synthesis of thin titania coatings onto the inner surface of quartz tubes and their photoactivity in decomposition of methylene blue and rhodamine b, Catalysts 11 (2021), https://doi.org/10.3390/catal11121538.
[48] B.H. Toby, R.B. Von Dreele, GSAS-II: the genesis of a modern open-source all purpose crystallography software package, J. Appl. Cryst. 46 (2013) 544–549.
[49] Y. Zeng, X. Tu, Plasma-catalytic hydrogenation of CO2 for the cogeneration of CO and CH4 in a dielectric barrier discharge reactor: Effect of argon addition, J. Phys. D. Appl. Phys. 50 (2017), https://doi.org/10.1088/1361-6463/aa64bb.
[50] V.T.T. Ho, D.H. Chau, K.Q. Bui, N.T.T. Nguyen, T.K.N. Tran, L.G. Bach, S. N. Truong, A High-Performing Nanostructured Ir Doped-TiO2 for Efficient Photocatalytic Degradation of Gaseous Toluene, Inorganics 10 (2022), https://doi.org/10.3390/inorganics10030029.
[51] T. Kozàk, A. Bogaerts, Splitting of CO2 by vibrational excitation in non-equilibrium plasmas: A reaction kinetics model, Plasma Sources Sci. Technol. 23 (2014), https://doi.org/10.1088/0963-0252/23/4/045004.
[52] G.Y. Fan, L. Zhang, H.Y. Fu, M.L. Yuan, R.X. Li, H. Chen, X.J. Li, Hydrous zirconia supported iridium nanoparticles: An excellent catalyst for the hydrogenation of haloaromatic nitro compounds, Catal. Commun. 11 (2010) 451–455, https://doi.org/10.1016/j.catcom.2009.11.021.
[53] M.J. Sharif, P. Maity, S. Yamazoe, T. Tsukuda, Selective hydrogenation of nitroaromatics by colloidal iridium nanoparticles, Chem. Lett. 42 (2013) 1023–1025, https://doi.org/10.1246/cl.130333.
[54] S. He, L. Xie, M. Che, H.C. Chan, L. Yang, Z. Shi, Y. Tang, Q. Gao, Chemoselective hydrogenation of α,β-unsaturated aldehydes on hydrogenated MoOx nanorods supported iridium nanoparticles, J. Mol. Catal. A Chem. 425 (2016) 248–254, https://doi.org/10.1016/j.molcata.2016.10.016.
[55] D. Robinson, R.W. Nicholls, Intensity measurements on the O2+ second negative, CO ångström and third positive and NO γ and β molecular band systems, Proc. Phys. Soc. 71 (1958) 957–964, https://doi.org/10.1088/0370-1328/71/6/308.
[56] M. Kraus, W. Egli, K. Haffner, B. Eliasson, U. Kogelschatz, A. Wokaun, Investigation of mechanistic aspects of the catalytic CO2 reforming of methane in a dielectric-barrier discharge using optical emission spectroscopy and kinetic modeling, Phys. Chem. Chem. Phys. 4 (2002) 668–675, https://doi.org/10.1039/b108040g.
[57] J. Ma, M.N.R. Ashfold, Y.A. Mankelevich, Validating optical emission spectroscopy as a diagnostic of microwave activated CH4 /Ar/ H2 plasmas used for diamond chemical vapor deposition, J. Appl. Phys. 105 (2009), https://doi.org/10.1063/1.3078032.
[58] X. Wang, Y. Gao, S. Zhang, H. Sun, J. Li, T. Shao, Nanosecond pulsed plasma assisted dry reforming of CH4: The effect of plasma operating parameters, Appl. Energy 243 (2019) 132–144, https://doi.org/10.1016/j.apenergy.2019.03.193.
[59] V. Pfeifer, T.E. Jones, J.J. Velasco Vélez, C. Massué, M.T. Greiner, R. Arrigo, D. Teschner, F. Girgsdies, M. Scherzer, J. Allan, M. Hashagen, G. Weinberg, S. Piccinin, M. Hävecker, A. Knop-Gericke, R. Schlögl, The electronic structure of iridium oxide electrodes active in water splitting, Phys. Chem. Chem. Phys. 18 (2016) 2292–2296, https://doi.org/10.1039/c5cp06997a.
[60] V. Pfeifer, T.E. Jones, J.J. Velasco Vélez, C. Massué, R. Arrigo, D. Teschner, F. Girgsdies, M. Scherzer, M.T. Greiner, J. Allan, M. Hashagen, G. Weinberg, S. Piccinin, M. Hävecker, A. Knop-Gericke, R. Schlögl, The electronic structure of iridium and its oxides, Surf. Interface Anal. 48 (2016) 261–273, https://doi.org/10.1002/sia.5895.
[61] F. Bernardi, J.D. Scholten, G.H. Fecher, J. Dupont, J. Morais, Probing the chemical interaction between iridium nanoparticles and ionic liquid by XPS analysis, Chem. Phys. Lett. 479 (2009) 113–116, https://doi.org/10.1016/j.cplett.2009.07.110.
[62] E. Willinger, C. Massué, R. Schlögl, M.G. Willinger, Identifying Key Structural Features of IrOx Water Splitting Catalysts, J. Am. Chem. Soc. 139 (2017) 12093–12101, https://doi.org/10.1021/jacs.7b07079.
[63] S. Geiger, O. Kasian, B.R. Shrestha, A.M. Mingers, K.J.J. Mayrhofer, S. Cherevko, Activity and Stability of Electrochemically and Thermally Treated Iridium for the Oxygen Evolution Reaction, J. Electrochem. Soc. 163 (2016) F3132–F3138, https://doi.org/10.1149/2.0181611jes.
[64] Y. Lu, J. Wang, L. Yu, L. Kovarik, X. Zhang, A.S. Hoffman, A. Gallo, S.R. Bare, D. Sokaras, T. Kroll, V. Dagle, H. Xin, A.M. Karim, Identification of the active complex for CO oxidation over single-atom Ir-on-MgAl2O4 catalysts, Nat. Catal. 2 (2019) 149–156.
[65] B. Eliasson, U. Kogelschatz, B. Xue, L.M. Zhou, Hydrogenation of carbon dioxide to methanol with a discharge-activated catalyst, Ind. Eng. Chem. Res. 37 (1998) 3350–3357, https://doi.org/10.1021/ie9709401.
[66] B. Ashford, C.K. Poh, K. (Ken) Ostrikov, L. Chen, X. Tu, Plasma-catalytic CO2 hydrogenation to ethane in a dielectric barrier discharge reactor, J. CO2 Util. 57 (2022) 101882, https://doi.org/10.1016/j.jcou.2022.101882.